Lawrence Berkeley National Laboratory
Advanced Light Source

Title
Photon-counting MCP/Timepix detectors for soft X-ray imaging and spectroscopic applications

Permalink
https://escholarship.org/uc/item/2463h9v4

Journal
Journal of Synchrotron Radiation, 28(4)

ISSN
0909-0495

Authors
Tremsin, Anton S
Vallerga, John V
Siegmund, Oswald HW
et al.

Publication Date
2021-07-01

DOI
10.1107/s1600577521003908

Peer reviewed

eScholarship.org Powered by the California Digital Library
University of California

ARTICLE IN PRESS – J. Synchrotron Rad.

JOURNAL OF SYNCHROTRON RADIATION

ISSN 1600-5775

Photon-counting MCP/Timepix detectors for soft X-ray imaging and spectroscopic applications

Proof instructions

Proof corrections should be returned by **14 May 2021**. After this period, the Editors reserve the right to publish your article with only the Managing Editor's corrections.

Please
(1) Read these proofs and assess whether any corrections are necessary.
(2) Check that any technical editing queries highlighted in **bold underlined** text have been answered.
(3) Send corrections by e-mail to **tw@iucr.org**. Please describe corrections using plain text, where possible, giving the line numbers indicated in the proof. Please do not make corrections to the pdf file electronically and please do not return the pdf file. If no corrections are required please let us know.

To arrange payment for **open access**, please visit **https://scripts.iucr.org/openaccess/?code=gy5020**. To purchase printed offprints, please complete the attached order form and return it by e-mail.

Please check the following details for your article

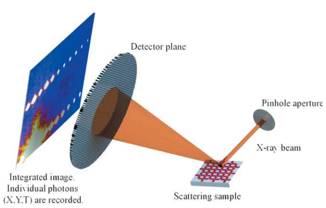

Thumbnail image for contents page

Synopsis: A photon-counting detector that employs microchannel plates combined with a quad Timepix readout is evaluated for soft X-ray imaging experiments conducted at synchrotron beamline facilities, where the time and position of each photon is registered by the detector. This work describes proof-of-principle experiments conducted with this technology where a spatial resolution of ~6 μm is achieved with single-photon counting. Future developments of this technology for the possible extension of X-ray photon correlation spectroscopy analysis to sub-microsecond timescales are presented.

Abbreviated author list: Tremsin, A.S. (iD 0000-0003-2443-7576); Vallerga, J.V.; Siegmund, O.H.W.; Woods, J.; De Long, L. E.; Hastings, J. T.; Koch, R. J.; Morley, S. A. (iD 0000-0001-8197-2431); Chuang, Y.-D. (iD 0000-0002-2773-3840); Roy, S.

Keywords: soft X-ray detectors; photon counting; microchannel plates; X-ray photon correlation spectroscopy; Timepix

Licence to publish: Licence to publish licence agreed.

How to cite your article in press

Your article has not yet been assigned page numbers, but may be cited using the doi:

Tremsin, A.S., Vallerga, J.V., Siegmund, O.H.W., Woods, J., De Long, L. E., Hastings, J. T., Koch, R. J., Morley, S. A., Chuang, Y.-D. & Roy, S. (2021). *J. Synchrotron Rad.* **28**, https://doi.org/10.1107/S1600577521003908.

You will be sent the full citation when your article is published and also given instructions on how to download an electronic reprint of your article.

Files: s/gy5020/gy5020.3d s/gy5020/gy5020.sgml **GY5020** FA IU-2113/34(7)5 2110/23(7)5 () GY5020 PROOFS S:FA:2021:28:4:0:0–0

JOURNAL OF SYNCHROTRON RADIATION

ISSN 1600-5775

Received 3 December 2020
Accepted 12 April 2021

Edited by A. Bergamaschi, Paul Scherrer Institut, Switzerland

Keywords: soft X-ray detectors; photon counting; microchannel plates; X-ray photon correlation spectroscopy; Timepix.

Photon-counting MCP/Timepix detectors for soft X-ray imaging and spectroscopic applications

Anton S. Tremsin,[a]* John V. Vallerga,[a] Oswald H.W. Siegmund,[a] Justin Woods,[b] Lance E. De Long,[c] Jeffrey T. Hastings,[c] Roland J. Koch,[d] Sophie A. Morley,[d] Yi-De Chuang[d] and Sujoy Roy[d]

[a]Space Sciences Laboratory, University of Kentucky, Lexington, KY 40506, USA, [b]Department of Physics and Astronomy, University of Kentucky, Lexington, KY 40506, USA, [c]Department of Electrical and Computer Engineering, Lawrence Berkeley National Laboratory, 1 Cyclotron Road, Berkeley, CA 94720, USA, and [d]Advanced Light Source, Lawrence Berkeley National Laboratory, 1 Cyclotron Road, Berkeley, CA 94720, USA. *Correspondence e-mail: ast@ssl.berkeley.edu

Detectors with microchannel plates (MCPs) provide unique capabilities to detect single photons with high spatial (<10 µm) and timing (<25 ps) resolution. Although this detection technology was originally developed for applications with low event rates, recent progress in readout electronics has enabled their operation at substantially higher rates by simultaneous detection of multiple particles. In this study, the potential use of MCP detectors with Timepix readout for soft X-ray imaging and spectroscopic applications where the position and time of each photon needs to be recorded is investigated. The proof-of-principle experiments conducted at the Advanced Light Source demonstrate the capabilities of MCP/Timepix detectors to operate at relatively high-input counting rates, paving the way for the application of these detectors in resonance inelastic X-ray scattering and X-ray photon correlation spectroscopy (XPCS) applications. Local count rate saturation was investigated for the MCP/Timepix detector, which requires optimization of acquisition parameters for a specific scattering pattern. A single photon cluster analysis algorithm was developed to eliminate the charge spreading effects in the detector and increase the spatial resolution to subpixel values. Results of these experiments will guide the ongoing development of future MCP devices optimized for soft X-ray photon-counting applications, which should enable XPCS dynamics measurements down to sub-microsecond timescales.

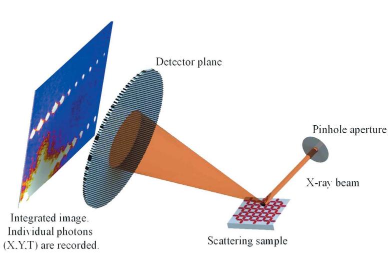

1. Introduction

The recent development of novel techniques enabled by the combination of bright partially coherent X-ray sources and advanced X-ray detectors provides experimental capabilities to study various microscopic dynamic phenomena. X-ray photon correlation spectroscopy (XPCS) is a technique that can probe the dynamics of complex systems at length scales in the Ångstrom range (Dierker *et al.*, 1995; Mochrie *et al.*, 1997; Grübel *et al.*, 2008; Sinha *et al.*, 2014; Shpyrko, 2014; Sandy *et al.*, 2018). The scattered X-ray radiation reflects the microscopic morphology of the sample. The dynamics of that morphology are represented by changes in the intensity of the speckle patterns. These can vary over a very wide range of timescales, from seconds to picoseconds depending on the physical system under investigation. The large dynamic range introduces very stringent requirements on the detection systems needed for such experiments. The speckle patterns need to be measured with very high timing and sufficient angular or scattering momentum (q) resolution.

The advent of diffraction limited light sources (*e.g.* ALS-U, APS-U, https://als.lbl.gov/als-u/resources/; https://www.ap-

Files: s/gy5020/gy5020.3d s/gy5020/gy5020.sgml GY5020 FA IU-2113/34(7)5 2110/23(7)5 () GY5020 PROOFS S:FA:2021:28:4:0:0–0

s.anl.gov/APS-Upgrade) and free-electron laser X-ray sources (LCLS-II, Galayda, 2018) has substantially increased the intensity of coherent X-rays available for experiments. The development of detectors, which can meet the requirements for spatial and timing resolution while at the same time facilitate operation in a large dynamic range, is crucial for using ultra-high fluxes for XPCS experiments. At the same time, the spatial resolution and detection efficiency of soft X-ray detectors in resonant inelastic X-ray scattering (RIXS) experiments (Rossi *et al.*, 2019) in many cases determine the ultimate resolution of these experiments. Therefore the development of soft X-ray detectors with high spatial and temporal resolution capable of operation at high counting rates with high detection efficiency is very important for future operation at various synchrotron sources.

Fast non-imaging and linear detectors can be used for XPCS experiments, *e.g.* 1D Mythen devices (Westermeier *et al.*, 2013). However, they introduce substantial constraints on the phenomena that can be studied, require relatively long illumination leading to radiation damage of materials under investigation and are difficult to use when the alignment to a specific speckle becomes problematic. Furthermore, they are restricted to one speckle (or a few speckles in the case of 1D arrays) at a time, whereas complex systems typically exhibit multiple different speckles with various 2D distributions. In addition, the XPCS time resolution scales **are** the inverse square root of the number of speckles used in the analysis; therefore, high timing resolution detectors with full 2D imaging capabilities are needed for these experiments.

A number of fast X-ray 2D area detectors have been developed recently for XPCS experiments where the intensity of the incoming X-ray specular reflection pattern is measured with sub-millisecond timing resolution (Denes *et al.*, 2009; Johnson *et al.*, 2012; Becker *et al.*, 2013, 2020; Pennicard *et al.*, 2013; Hatsuia & Graafsma, 2015; Zhang *et al.*, 2016, 2018; Rumaiz *et al.*, 2016; Kleczek *et al.*, 2018; Graafsma *et al.*, 2020). Most of these devices are built for moderate-to-high X-ray energies, exceeding ~10 keV. In this work we concentrate on the development of detectors for soft XPCS experiments, where detection technology at present does not allow investigation of fluctuations at the nanometre length scale with a sub-microsecond time resolution. Integrating soft X-ray detectors, such as charge coupled devices (CCDs), have excellent detection efficiency but limited timing resolution from tens to hundreds of microseconds at present (*e.g.* Denes *et al.*, 2009). For fast hybrid detectors, where incoming photons are converted to a charge in Si or other solid-state sensors and subsequently registered by a readout-specific integrated circuit (ROIC), such as event counting Medipix/Timepix, integrating AGIPD devices (Graafsma *et al.*, 2020) have a minimum charge threshold value corresponding to a photon energy of several kiloelectron volts. Detection of soft X-ray photons (~100 eV to ~1.2 keV) therefore requires charge amplification. We accomplish this by employing vacuum electron multipliers such as microchannel plates (MCPs).

Detectors with microchannel plates have been used for soft X-ray and UV photon counting for a number of years, primarily for astrophysical instrumentation and applications where incoming fluxes are relatively low. However, recent progress in MCP detectors has extended their photon-counting capabilities to relatively high counting rates exceeding $\sim 10^8$ photons s^{-1} (Tremsin *et al.*, 2020*a*,*b*) and allowed the detection of many photons simultaneously. The quantum efficiency (QE) of MCP detectors for soft X-ray photons is determined by the efficiency of the photon conversion into photoelectrons by a particular photocathode, which can be deposited directly onto the MCP input side (Fraser, 1983; Siegmund *et al.*, 1988; Tremsin & Siegmund, 2005). Generally, the detection efficiency of MCP devices is not as high as the efficiency of soft X-ray CCD detectors. However, their intrinsic timing resolution, being as low as ~10–25 ps (Martindale *et al.*, 2007; Vredenborg *et al.*, 2008; Va'vra *et al.*, 2009), and sub-20 µm spatial resolution (Bellazzini *et al.*, 2008; Siegmund *et al.*, 2009; Tremsin *et al.*, 2012) make these detectors very attractive for future soft RIXS and XPCS applications. In Section 2 we briefly describe how the MCP detectors with cross delay line (XDL) readout, widely used now for soft X-ray experiments, can be optimized for the photon-counting applications where low-intensity spots need to be measured in the presence of spatially separated bright areas. The main purpose of this study is the evaluation of the existing MCP detector configuration with Timepix readout (Llopart *et al.*, 2007) specifically for RIXS and XPCS applications in the soft X-ray regime. We discuss the near-future potential of this technology with an emphasis on the new generation of Timepix readout devices. The proof-of-principle measurements conducted at the COSMIC scattering beamline 7.0.1.1 at the Advanced Light Source described in Section 4 demonstrate the strengths and deficiencies of the existing MCP detection technology. The results presented in this paper lay the foundations for future improvements of this detection technology. The ongoing upgrade to next-generation Timepix readouts, the existing Timepix3 (Poikela *et al.*, 2014) and the latest Timepix4 ROIC will substantially enhance the capabilities of MCP/Timepix detectors for soft RIXS, XPCS and other experiments.

2. Soft X-ray MCP detectors with XDL and Timepix readouts

Detectors using MCPs are capable of single-particle detection with high spatial and temporal resolution due to high gain (with a factor of up to $\sim 10^7$) electron multiplication within the MCP pores, with jitter times as small as ~10 ps without signal spread beyond the MCP pore (Wiza, 1979; Martindale *et al.*, 2007; Vredenborg *et al.*, 2008; Va'vra *et al.*, 2009). To detect photons, the incoming flux of the soft X-rays has to be converted into photoelectrons by a photocathode before these photoelectrons are amplified in the microchannels. The efficiency of this conversion determines the quantum detection efficiency (QDE) of the entire device, as the probability of every photoelectron to create a charge avalanche in the microchannel is close to unity. No ideal photocathode exists for all photon energies and the selection of specific photo-

Files: s/gy5020/gy5020.3d s/gy5020/gy5020.sgml GY5020 FA IU-2113/34(7)5 2110/23(7)5 () GY5020 PROOFS S:FA:2021:28:4:0:0–0

cathode materials and geometry can only be performed for a given wavelength range. Various soft X-ray photocathodes have been developed for the MCP detectors, with alkali halide films being widely used for soft X-ray photon conversion (*e.g.* KBr or CsI photocathodes, Fraser, 1983; Siegmund *et al.*, 1988). In this study, we use a conventional KBr opaque photocathode evaporated directly on the input surface of the MCP chevron stack.

The main subject of this paper is the optimization of the detector readout for the experiments where timing and position of each photon need to be detected, including multiple simultaneous event detection. Two readout technologies are considered for the use within MCP detectors: a cross delay line (XDL) readout (Siegmund *et al.*, 1999; Tremsin *et al.*, 2007*a*) and bare Timepix ROICs (Llopart *et al.*, 2007) are placed directly behind the MCP stack. The schematics of these two detector configurations are shown in Figs. 1 and 2. There is not a single readout type that can fulfil the requirements for all experiments; therefore, an optimal readout needs to be chosen for a specific experiment (Tremsin *et al.*, 2020*a*). XDL detectors have excellent linearity, great timing (<50 ps) and spatial (<20 μm) resolution, and large active areas (exceeding 10 cm × 10 cm), but they cannot register multiple near-simultaneous events. They also have a limit on the input counting rates, typically below ~1 MHz per entire detector area, and a limited lifetime due to the ageing of the MCP from operations at very high gain settings (10^6–10^7 e^- $photon^{-1}$). On the other hand, an MCP electron amplifier combined with a Timepix readout can operate at very high input rates exceeding ~100 MHz and can detect many particles simultaneously. The timing resolution is limited to 10 ns for the first-generation Timepix (Llopart *et al.*, 2007) and is improved to ~1.6 ns for Timepix3 devices (Poikela *et al.*, 2014) and anticipated to be ~200 ps for the Timepix4 ROIC. Although the experimental results presented in this paper were obtained with Timepix readouts, multiple aspects of MCP/Timepix operation and optimization (*e.g.* charge collection by bare Timepix chips, thermal load management, charge spread over multiple pixels,

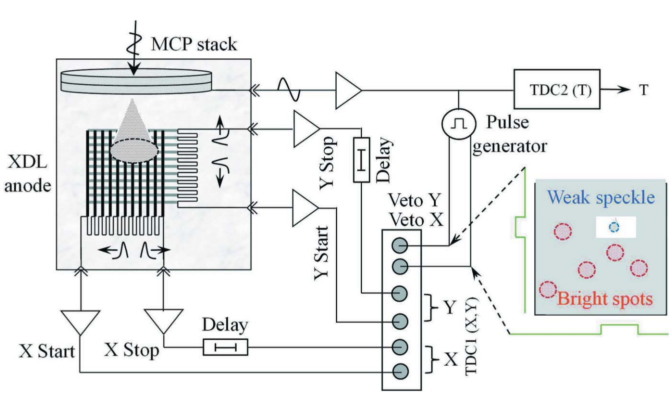

Figure 1
Schematic of the XDL event counting detector with MCPs. The position of each particle is encoded by two orthogonal delay lines, and the timing of the particle is picked up at the MCP output electrode. Custom TDCs with the possibility to veto signals are used for the selection of the region of interest in order to avoid global count rate saturation of the readout electronics.

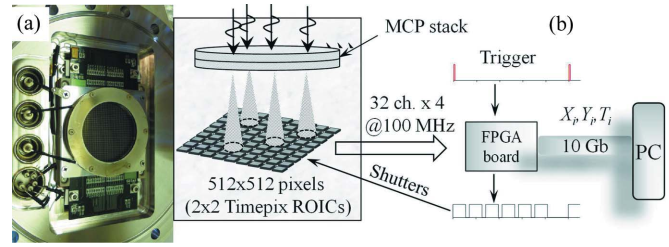

Figure 2
(*a*) Photograph and (*b*) schematic of the MCP detector with 2 × 2 array of Timepix readout used in the experiments. The open-face detector is mounted under vacuum on an 8 inch flange as shown in (*a*). The detector active area of 28 mm × 28 mm is located behind the circular mesh grid visible in the image. The detector signals are transferred outside the vacuum over 128 parallel lines and are processed by a custom FPGA data processing board. An external trigger can be used to generate the sequence of acquisition frames, each controlled to a 10 ns timing accuracy. The time of photon arrival within each of these frames is measured by the Timepix readout. Due to the use of frame-based Timepix readout, only one photon per acquisition frame is possible for the current detector, whereas next-generation readouts (Timepix3 and Timepix4) can operate in event driven mode to remove the latter limitation on the detector local count rate.

MCP count rate saturation and others) will directly benefit the development of future detectors with Timepix3 and Timepix4 readouts. Despite the fact that certain limitations exist for the first-generation Timepix readout used in this study, the unique capabilities of these detectors to operate at high counting rates with low MCP gain and detect multiple simultaneous particles with sub-10 μm spatial resolution at high dynamic range, the absence of readout noise and the low dark count rate make these devices attractive for various soft X-ray imaging applications at synchrotron beamlines.

2.1. Optimization of MCP/XDL detectors for high input rates

One of the main deficiencies of MCP/XDL detectors in XPCS applications is their inability to detect multiple particles simultaneously and the limit on the maximum detection count rate. In XPCS experiments, for example, the incoming flux consists of very bright illumination in a small area (*e.g.* Bragg diffraction spots, specular reflected spots) and very weak speckles directly next to them. The dead time related to single-photon processing means that the detection of photons in weak speckles can be substantially suppressed by the unwanted bright spots. Although detection methods for several near-simultaneous particles have been developed (Jagutzki *et al.*, 2002), signals corresponding to separate particles still need to be distinguished at the timing output channel of the detector, as shown in Fig. 1. The timing of photons in this detector configuration is reconstructed by measuring the pulse at the MCP output electrode. The signal propagation along the back electrode is far from ideal for fast timing measurements; therefore, photons still need to be well separated in time, which can be problematic for experiments involving fast dynamic systems. Provided the photons are distinguishable by the time-processing electronics, one of the possible optimizations of MCP/XDL detectors operating at high input fluxes is the application of gating implemented at

Files: s/gy5020/gy5020.3d s/gy5020/gy5020.sgml GY5020 FA IU-2113/34(7)5 2110/23(7)5 () GY5020 PROOFS S:FA:2021:28:4:0:0–0

the processing electronics. We have already reported how gating of the time-to-digital converter (TDC) can be implemented for time-of-flight experiments in the case of angle-resolved photoemission spectroscopy (ARPES) (Tremsin *et al.*, 2007*b*). In those experiments, the unwanted bright peak from secondary electrons in the time distribution can be ignored, thus avoiding the suppression of weak peaks by the detector dead time. A similar TDC gating can be implemented for the experiments where the registration of a weak speckle is required in the presence of other unwanted bright spots. Only photons corresponding to a given area will trigger the processing electronics in such a detector configuration, where the TDC ignores all events except in a pre-selected area of the detector as depicted schematically in Fig. 1. Two veto pulses are generated for X and Y channels by a pulse generator triggered by the MCP out channel. This approach clearly requires preliminary measurements with an ungated full field of view in order to determine the location of the area of interest.

2.2. MCP detectors with Timepix readout

The unique capability to detect many near-simultaneous events by combining an MCP with a Timepix readout device is possible due to the fact that each pixel in the detector readout can register an event almost independently from other pixels. Furthermore, the MCP/Timepix detectors can operate at a relatively low gain compared with other readouts owing the intrinsic electronic noise in a pixel of the Timepix readout chip, which is approximately ~50–75 e^- r.m.s. Consequently, the low-level threshold of Timepix can be set to ~1000 electrons. Depending on how many pixels are excited by a single photon, the gain in the MCP/Timepix detector can be set to as low as 10^4 e^- photon^{-1}. Direct placement of the Timepix chip behind the MCP eliminates any transfer of charge or analog signals, and only the digital values are read from the Timepix chip into the data processing FPGA board, as shown in Fig. 2. In the present study, we used first-generation Timepix chips; these impose a certain limitation to applications where the timing of each photon needs to be detected with an accuracy better than ~1 ms. This limitation is related to the fact that only one photon can be detected per pixel per acquisition frame, which needs to be followed by a 320 µs readout dead time; the first-generation Timepix is still a frame-based readout. The next-generation Timepix3 and Timepix4 readout chips are capable of pixel-based event-driven operation, thus eliminating such deficiency and enabling the uninterrupted detection of X-ray photons. However, many of the characteristics stemming from the combination of MCPs with the Timepix readout are common to all generations of Timepix readouts and therefore are tested and optimized in the present study. These characteristics are: (i) number of pixels excited per individual photon, (ii) local MCP gain saturation, (iii) spatial resolution, (iv) detection efficiency, (v) detector operation parameters such as gain, accelerating the field between the MCP and Timepix. The capability of these devices to simultaneously register bright and dim spots, where the difference in their flux is more than three orders of magnitude, is demonstrated by our proof-of-principle experiments described in Section 4.

The MCP/Timepix detector used in the present study has a relatively small active area. The original Timepix chips require a wire-bonded connection on one side. Only 2N (where N is an integer) chip tiling configurations are possible without large dead areas, limiting the size of one side of the active area to 28 mm. Moreover, there is a small gap in between the chips, which is typically ~150 µm in our current devices. The through silicon via (TSV) technology will be implemented in Timepix4 devices, which will also feature a larger single-chip size (~28 mm × 24 mm) to provide larger active areas in future work. The MCP/Timepix detectors also require carefully designed heat transfer and dissipation outside the vacuum chamber as substantial power is generated by Timepix chips (up to 1 W cm^{-2}).

3. Experimental setup

The results reported in this paper were obtained with a detector containing a chevron stack of MCPs with 6 µm pores, 50 mm in diameter, 0.3 mm thickness with 8° pore bias (tilt of the pores relative to the MCP normal) and ~50 MΩ resistance per MCP. An ~1 µm-thick KBr photocathode was evaporated on the input surface of the top MCP, which improves the QDE of the detector to 30–70% (Siegmund *et al.*, 1988) depending on the photon wavelength. A quad assembly of bare Timepix chips was placed behind the MCP stack. Custom-built readout electronics were used to control and receive data from the Timepix chip over 128 parallel readout lines operating at 100 MHz (Tremsin *et al.*, 2015, 2020*a*). The first-generation Timepix readout operates in frame-based mode, where the time of arrival of photons in relation to the time of the frame is recorded in each individual pixel. Only the first photon per pixel per frame can be detected. The global detector readout time is ~320 µs, enabling a maximum rate of ~1200 frames s^{-1}. The duty cycle of the detector, *i.e.* readout dead time versus sensitive time, is determined by the time of the acquisition shutter as the readout dead time is fixed. Here we implemented ~9.68 ms and ~1.1 ms shutter time lengths, which equate to acquisition duty cycles of 95% and 76% for these two shutter values, respectively. An external pulse generator was used to trigger the detector for both these modes, as shown in Fig. 3. A list of photon events in the form of XYT (pixel indices X and Y and photon time T relative to the free-running 100 MHz global clock counter in the FPGA processing board) was saved to a disk in the data acquisition computer for subsequent analysis. Most photon events activated more than one pixel on the Timepix readout due to charge spreading in the gap between the MCP and Timepix chips. A specific data processing procedure was developed to assign only one pixel per event, and this procedure will be described in Section 4.1. The time of photon arrival was recorded with 1.28 µs and 160 ns binning for ~9.68 ms and ~1.1 ms shutter widths, respectively. The detector was mounted on an 8 inch conflat flange attached to the scattering

Files: s/gy5020/gy5020.3d s/gy5020/gy5020.sgml GY5020 FA IU-2113/34(7)5 2110/23(7)5 () GY5020 PROOFS S:FA:2021:28:4:0:0–0

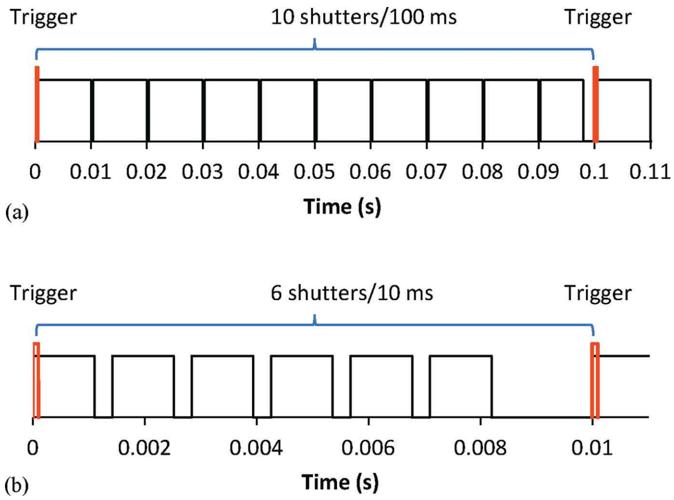

Figure 3
Timing diagrams of the two acquisition frame configurations used in our experiments. An external pulse generator provided the trigger signal to the FPGA board, which generated ten acquisition frames for the 10 Hz trigger, configuration (*a*), and six acquisition frames for a 100 Hz trigger, configuration (*b*). The detector dead time (frame readout) of 320 µs was fixed for both configurations, while the length of the acquisition shutter was 9.68 ms for configuration (*a*) and 1.1 ms for configuration (*b*). A larger dead-time gap occured between the last shutter and next trigger (2 ms and 1.8 ms for 10 Hz and 100 Hz, respectively). Time of photon arrivals was registered with 1.28 µs accuracy for configuration (*a*) and 160 ns for configuration (*b*).

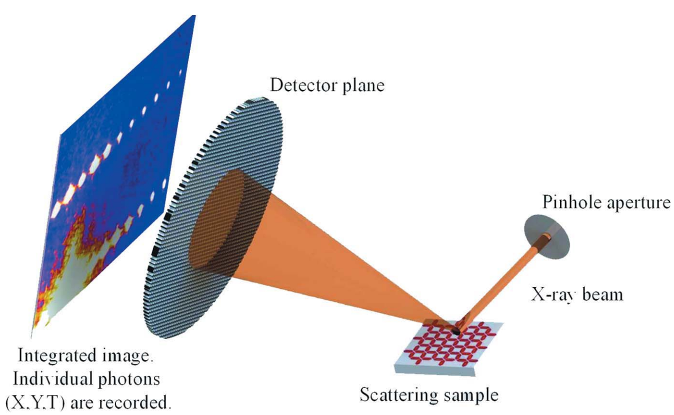

Figure 4
Schematic of XPCS setup at the COSMIC beamline at the Advanced Light Source, where the MCP/Timepix detector was installed.

endstation of the COSMIC beamline at the Advanced Light Source, Lawrence Berkeley National Laboratory. A monochromatic soft X-ray beam illuminated the sample at an incidence angle $\partial = 8.65°$, and the reflected/scattered photons were registered by the MCP/Timepix detector at an angle of $2\partial = 18°$, as shown in Fig. 4. The pinhole (7 µm in diameter) to filter out the coherent portion of the X-rays was located about 1 cm in front of the sample and the distance between the sample and the detector was set to 1 m.

The sample used in the present study was a square array of permalloy ($Ni_{0.8}Fe_{0.2}$) nanomagnets fabricated on a silicon wafer using electron-beam lithography (Chen *et al.*, 2019). The sample was capped with 1.5 nm of Al to guard against oxidation. The block-spin dimensions were 470 nm long, 170 nm wide and 3 nm thick with a lattice constant a = 600 nm. The thickness of the permalloy was chosen so that the array undergoes fluctuation and settles into an antiferromagnetic ground state near room temperature. RIXS produces both structural Bragg peaks and antiferromagnetic Bragg peaks at the detector.

4. Results and discussion

In our experiments, we varied the temperature of the sample while it was illuminated by a monochromatic coherent X-ray beam at 708 eV (Fe L_3-edge). A typical full-field image registered by the MCP/Timepix detector is shown in Fig. 5, which contains both Bragg diffraction spots from an artificial spin ice lattice and antiferromagnetic Bragg peaks (Woods *et*

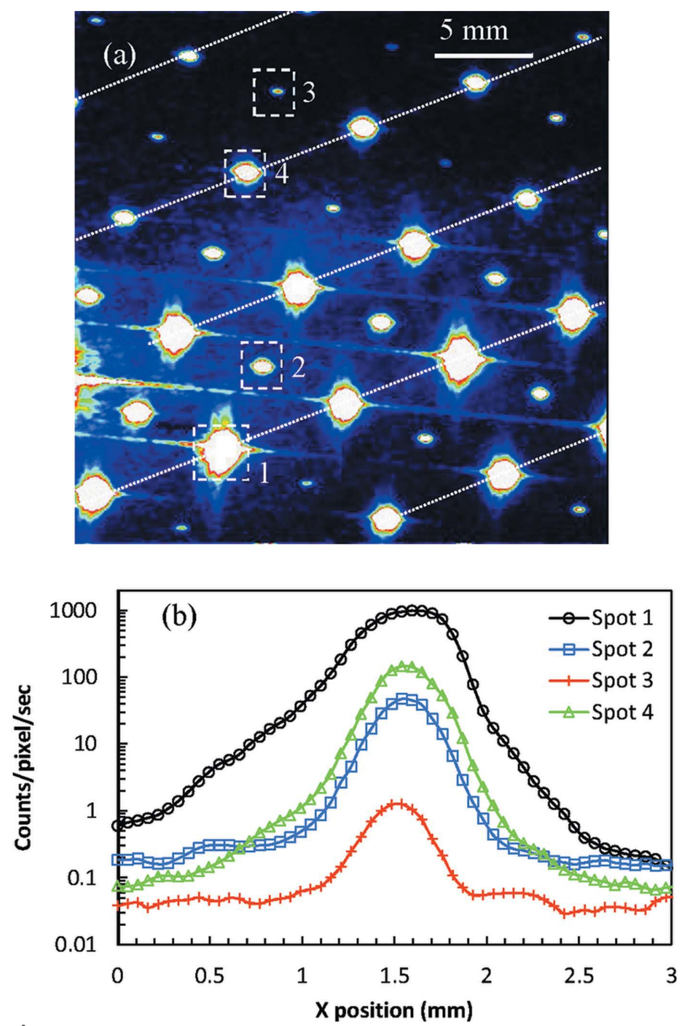

Figure 5
(*a*) Typical raw image acquired by the MCP/Timepix detector during XPCS experiments. All photons registered within 1000 s are summed in the image, while the time and position of each photon was recorded during the measurement. (*b*) Linecut taken along the *x* direction through Spots 1–4 outlined by dashed rectangles in (*a*). The count rate within different spots in the image varies by more than three orders of magnitude. The Bragg diffraction spots from an artificial spin ice lattice are marked by dashed lines. The remaining spots correspond to antiferromagnetic Bragg peaks.

Files: s/gy5020/gy5020.3d s/gy5020/gy5020.sgml **GY5020** FA IU-2113/34(7)5 2110/23(7)5 () GY5020 PROOFS S:FA:2021:28:4:0:0–0

Table 1
Size and input count rate for the spots indicated by dashed rectangles in Fig. 5.

	Spot 1	Spot 2	Spot 3	Spot 4
Area (pixels)	1570	497	193	726
Input count rate (photons s^{-1})	16000	242	7.7	941

al., 2021). The brightest specular reflection spot is just to the left of the field of view, not interfering with the signal of interest. As mentioned earlier, these experiments require detection of incoming photons with a very large dynamic range, where bright spots can possibly inhibit the detection of dim speckles of interest. The full parallel processing of events by each pixel in an MCP/Timepix detector is one of the crucial characteristics of these devices, which extend the capabilities of MCP detectors originally developed for low-flux particle counting. Cross sections through several spots in that image, shown in Fig. 5(*b*), indicate that the intensity in the spots varied by more than three orders of magnitude. The input flux and the size of the illuminated area for these spots are described in Table 1. Although our MCP/Timepix detector can count the number of registered photons at rates exceeding 100 MHz per detector chip, the timing of each individual photon can only be measured at lower rates due to the limitation of the current Timepix readout, as described earlier. The individual single-frame images acquired in our experiment with the acquisition frame lengths of 9.68 ms and 1.1 ms are shown in Fig. 6. The colour in these images represents the time of photon arrival within the shutter in microseconds. These single-frame images contain all pixels activated by the charge generated by the MCP stack. In most cases, one photon activates several pixels due to charge spread behind the MCP stack. However, in some photon-counting experiments (*e.g.* XPCS), ideally we need to determine the correct location and time of one incoming photon rather than the footprint of an amplified electron cloud, *i.e.* we need to select only one pixel per photon. The process of data reduction, assigning only one pixel per incoming photon, is described in the next section.

4.1. Cluster analysis: single pixel per photon

Optimizing the size of the electron cloud generated by the MCP to the pixel size of the Timepix chip can be achieved by changing the MCP gain, the accelerating voltage and the gap distance between the MCP and the Timepix chip. Most MCP detectors operate in a saturated mode, where the gain of individual events has a relatively small variation (typically $\pm 25\%$) around the modal gain value. That is achieved usually at an MCP gain of 10^6–10^7 e^- photon^{-1}. We operate the MCP stack at much lower gain and therefore do not achieve full saturation. On one hand, this allows operation of the MCP at much higher photon rates but, at the same time, it leads to a wider distribution of gain between individual photon events. As a result, the size of the electron cloud ejected from the MCP and therefore its footprint on the Timepix chip also changes from event to event. Optimization of MCP saturation

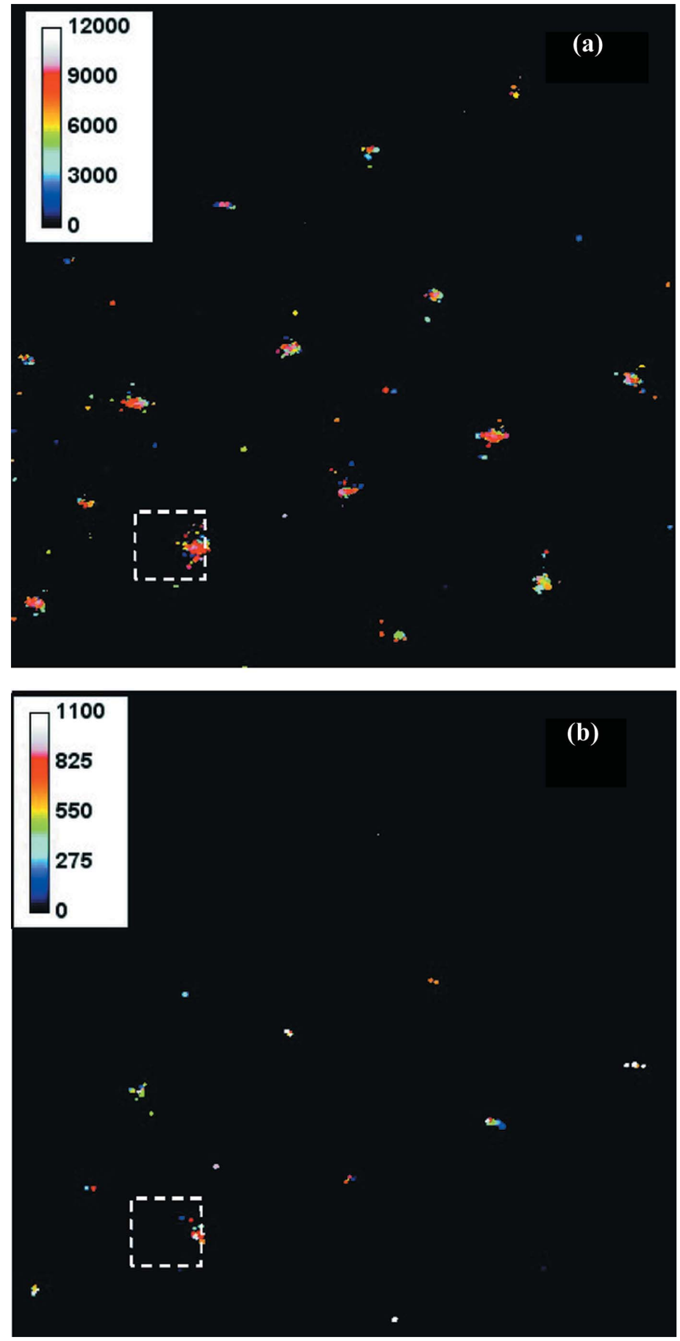

Figure 6
Single-frame images acquired by the MCP/Timepix detector. The colour represents the relative time of photon arrival (in microseconds) within the acquisition frame. (*a*) Frame length of 9.68 ms; (*b*) frame length of 1.1 ms. The dashed rectangles indicate the spots shown in more detail in Figs. 8 and 9.

at a relatively low gain of 10^4–10^5 will be explored in our near-future studies.

For experiments where single-pixel detection is required, we developed and implemented a data reduction procedure, which is schematically described in Fig. 7. This procedure is executed on each frame acquired by our detector and it can either be done in real time or post-experiment after all the raw data are recorded. The criteria by which the individual

Files: s/gy5020/gy5020.3d s/gy5020/gy5020.sgml **GY5020** FA IU-2113/34(7)5 2110/23(7)5 () GY5020 PROOFS S:FA:2021:28:4:0:0–0

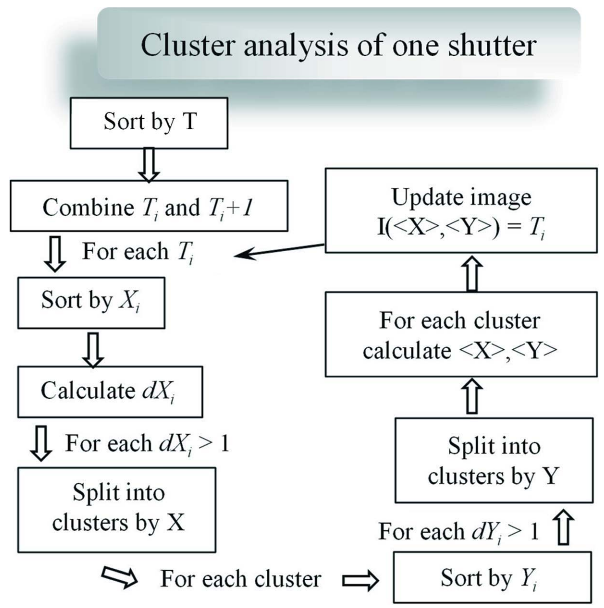

Figure 7
Schematic of the cluster analysis implemented in the raw photon list data in order to eliminate the effect of charge spreading within the MCP detector that results in multiple pixels excited by a single photon.

photons are identified are: (1) time of the photon arrival; (2) spatial separation of clusters in the x and y axes. For each individual frame, we sort the events by their time of arrival first and then combine those pixels, which differ only by one time-bin value. The exact length of a time bin can change from 10 ns to tens of microseconds, depending on the detector settings. This step is necessary since the neighbouring pixels excited by the same photon may have a different amount of accumulated charge, which leads to a small time difference for the threshold crossing between neighbouring pixels. When the event is close to the edge of the Timepix clock cycle, this leads to a different registered time by one time bin. In the second step, we separate the clusters with the same time of arrival by the gaps in their projections on the x and y axes and then calculate the centroid of the charge distribution for each event cluster to assign that event to a particular pixel. The result of this analysis for the spot indicated by the dashed rectangle in Fig. 6 is shown in Fig. 8 for a 9.68 ms acquisition frame and in Fig. 9 for a 1.1 ms frame. The shape of clusters in our raw data can be seen in Fig. 8(*a*)–9(*c*) and 9(*a*)–9(*c*). For this specific dataset, we found that, on average, each photon excited 5.3 pixels in our detector.

Cluster analysis not only reduces the raw data to one pixel and time per photon, but also improves the spatial resolution of the resulting dataset as the blurring from the charge spread is removed, as demonstrated in Fig. 10. The tilted rectangular grid pattern observed in these images is the shadow of a grid mesh installed in front of the MCP detector in order to enhance the detection efficiency by repelling the photoelectrons generated at the input surface back into the MCP pores. The shadow of the mesh (with a 1.27 mm period) becomes much sharper after cluster analysis. The spatial resolution of our dataset can be improved to sub-pixel level, which has been

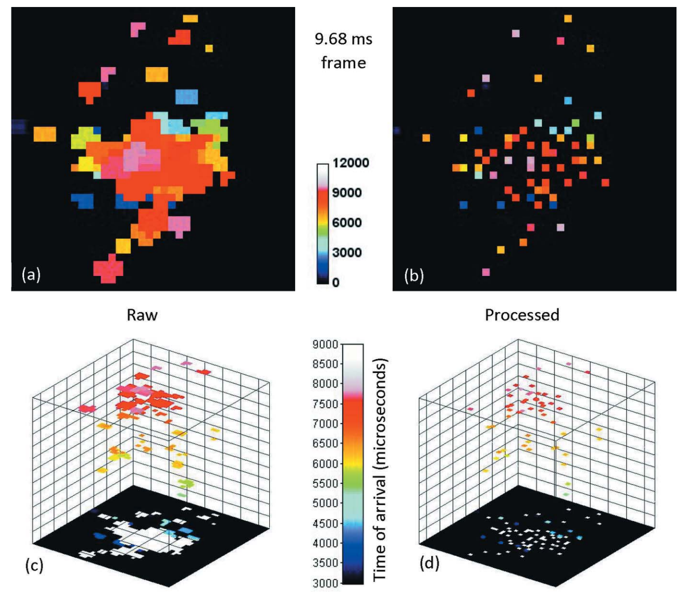

Figure 8
Detailed view on the photons registered within a single illumination spot indicated by the dashed rectangles in Fig. 6. The colour scale indicates the time of photon arrival in microseconds within the shutter. The time window for a single acquisition frame is 9.68 ms. (*a*) and (*c*) Raw image recorded by the MCP/Timepix detector showing multiple pixels excited at the Timepix readout by most photons. (*b*) and (*d*) The same acquisition frame processed by the developed cluster analysis tool. Only one pixel is assigned to each registered photon. Images (*c*) and (*d*) show a 3D representation of the measured data: the horizontal plane is the event position xy, and the vertical axis is the timing of the photon arrival (in microseconds).

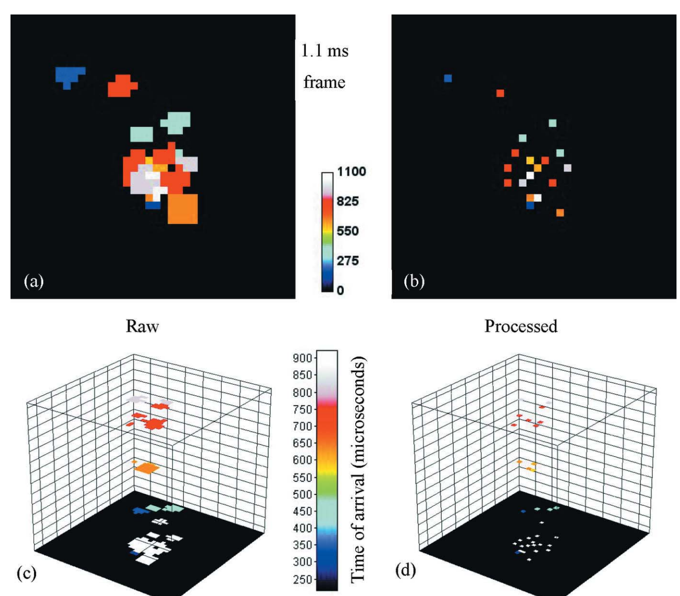

Figure 9
Detailed view on the photons registered within a single illumination spot indicated by the dashed rectangles in Fig. 6. The colour scale indicates the time of photon arrival in microseconds within the shutter. The time window for a single acquisition frame is 1.1 ms. (*a*) and (*c*) Raw image recorded by the MCP/Timepix detector showing multiple pixels excited at the Timepix readout by most photons. (*b*) and (*d*) The same acquisition frame processed by the developed cluster analysis tool. Only one pixel is assigned to each registered photon. Images (*c*) and (*d*) show a 3D representation of the measured data: the horizontal plane is the event position xy, and the vertical axis is the timing of the photon arrival (in microseconds).

Files: s/gy5020/gy5020.3d s/gy5020/gy5020.sgml **GY5020** FA IU-2113/34(7)5 2110/23(7)5 () GY5020 PROOFS S:FA:2021:28:4:0:0–0

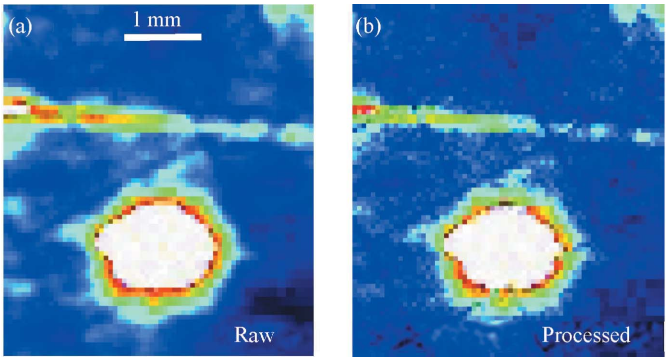

Figure 10
Zoomed-in area of the summed image acquired over 1000 s, shown in Fig. 5(*a*). The raw image (*a*) has lower spatial resolution due to blurring introduced by the charge spread in the MCP detector. (*b*) The same image after cluster analysis. The shadow of a grid mesh, installed in front of the detector, is resolved with 55 µm single-pixel resolution.

demonstrated previously (Suhling *et al.*, 1999; Vallerga *et al.*, 2005, 2011; Tremsin *et al.*, 2018). In Fig. 11 we demonstrate how a detector spatial resolution of ~6 µm can be achieved with event centroiding, which is important for some applications such as RIXS where the detector pixel resolution directly affects the RIXS spectral resolution. In real time, our data acquisition software performs the analysis of clusters [Figs. 11(*a*) and 11(*b*)] corresponding to individual photons and calculates the centre of each of these clusters to sub-pixel accuracy. The resulting 8192 × 8192 pixel image, a fragment of which is shown in Fig. 11(*c*), resolves individual pores of the top MCP, thus reaching the limit of possible resolution determined by the MCP geometry used in our detector (*i.e.* ~6 µm).

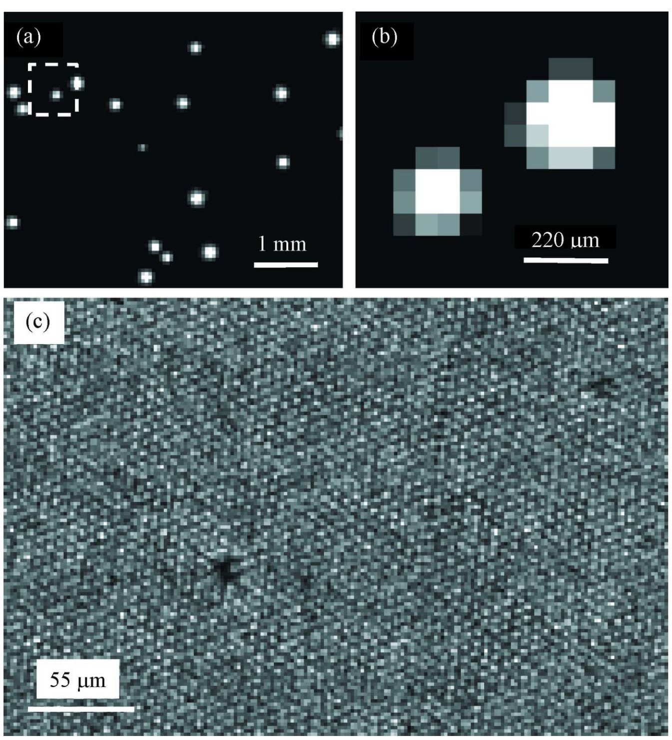

Figure 11
High spatial resolution photon detection through event centroiding. (*a*) Single-photon footprints detected by Timepix readout. (*b*) Enlargement of the area indicated by a dashed rectangle in (*a*), showing footprints of two photons in more detail. (*c*) Fraction of a high-resolution image obtained with full-field UV illumination of the MCP/Timepix detector. Individual pores of the MCP are resolved in the image. Two black spots correspond to the triple-point defects present in this MCP (crushed MCP pores at the points where three hexagonal multifibers meet).

4.2. Time of photon arrival: optimization of spot count rate and overlap correction

Once the subset of detected photons corresponding to the speckle(s) of interest is determined, the correlation analysis can be performed, provided that the time of photon arrival is accurately recorded by the detector. It is important that features reconstructed in this analysis originate from the sample and are not introduced by the experimental setup, especially not by the detector. In this section, we describe the deficiencies of present MCP/Timepix devices and how the input flux and detector acquisition configuration need to be optimized for XPCS experiments.

To extend the XPCS analysis to new time scales below milliseconds, preferably below microseconds and possibly into the nanosecond range, and to the limit of a single-photon quantum, it is not only the accuracy of photon detection that is important, but also the probability of photon detection over time, which should be constant to avoid introduction of unwanted features into the results of the XPCS analysis. In particular, periodic features create a strong signature in the two-time correlation function and must be avoided. An obvious challenge for many detection systems in that respect is the detector readout dead time when the detection efficiency drops to zero. For our current generation of MCP/Timepix detectors, we have a global dead time of 320 µs, which will be eliminated by the ongoing development of the MCP/Timepix3 event-driven system. To reduce the impact of the global dead time, the obvious choice is to run the acquisition with the highest duty cycle possible to minimize the missed photons during the dead time, advocating for the allowable long acquisition frames. On the other hand, the largest deficiency of our present system is the limitation of the first photon per pixel per frame, which requires the shortest achievable acquisition frames possible in order to have no pixels with more than one photon arriving within a single frame. Therefore, the length of the acquisition frame needs to be optimized for a particular illumination pattern and speckles of interest. In addition, the intensity of the speckles of interest should be as high as possible in order to probe dynamics in microseconds or even higher for the nanosecond scales to reach reasonable photon statistics for the XPCS analysis. It is difficult, if not impossible, to probe dynamics in microsecond and nanosecond scales if only a few photons arrive at the detector per speckle per second. At the same time, the number of speckles that can be observed simultaneously is limited by the detector spatial resolution and the size of the active area.

On the high side, there are two count-rate limitations to be considered: (i) the global count rate limitation, *i.e.* the number of photons that can be registered per entire detector area; (ii)

Files: s/gy5020/gy5020.3d s/gy5020/gy5020.sgml GY5020 FA IU-2113/34(7)5 2110/23(7)5 () GY5020 PROOFS S:FA:2021:28:4:0:0–0

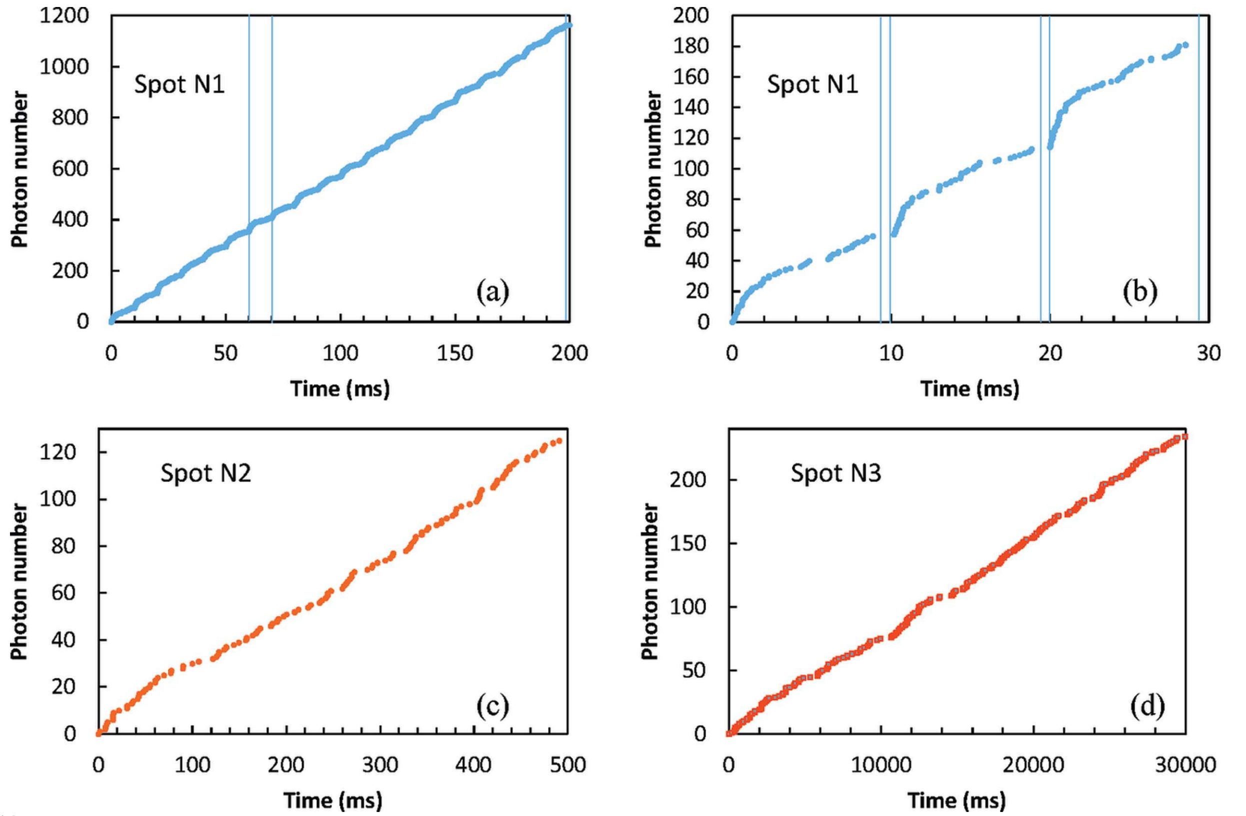

Figure 12
Time sequence of photons detected within Spots 1–3 indicated in Fig. 5(*a*). The *y* axis represents the consecutive photon number registered by the detector. The acquisition frame of 9.68 ms followed by the 0.32 ms readout time is shown in Fig. 3. Vertical lines in (*a*) and (*b*) indicate the boundaries of the acquisition frames. The cluster analysis was implemented in the raw data to represent each photon by only one pixel. The periodic structure seen in (*a*) and (*b*) is caused by the local count rate saturation in Spot 1 from the Timepix limitation of one pixel per frame in time-resolved counting mode. Some random variation of intensity within the spots N2 and N3 over a longer period of time seen in (*c*) and (*d*) can probably be attributed to the stability of the X-ray beam and the alignment on the sample.

the local count rate limitation, *i.e.* the number of photons detected per pixel or per speckle. The biggest challenge for our current MCP/Timepix detector setup is the local count rate limitation in timing mode with one photon per frame per pixel. Let us consider the time sequence of photons registered for spots with different illumination intensities: Spots 1–3 indicated in Fig. 5(*a*). We can clearly see in Figs. 12(*a*) and 12(*b*) that the intensity of Spot 1 has a very high modulation introduced by our detector readout triggered with a 10 ms repetition period. At the beginning of each acquisition frame, all pixels are available for photon detection and the consecutive number of acquired photons increases more rapidly at the beginning within each 10 ms period. Towards the end of the acquisition frame, many pixels are already busy processing prior photons and the probability, averaged over the whole detector, to detect photons at that time is reduced. This changes the slope of that curve. Obviously, detection of photons within Spot 1 is far from optimal and the detector local count rate saturation introduces a substantial modulation to the timing characteristics of detected photon flux within that spot. The lower flux within Spots 2 and 3 does not exhibit obvious modulations in the timing curves in Figs. 12(*c*) and 12(*d*), although some 100 Hz modulation of intensity is present for Spot 2 which we will show later in this section. To conclude, the intensity for 9.68 ms-wide frames is too high for Spot 1.

The histograms of time difference between consecutive photons for the same spots are shown in Fig. 13. The peak at ~2 ms seen in the histogram of Spot 1 can be attributed to the timing of our acquisition shutters: at the end of the 10-frame sequence shown in Fig. 3(*a*) there is a 2 ms gap, which can be

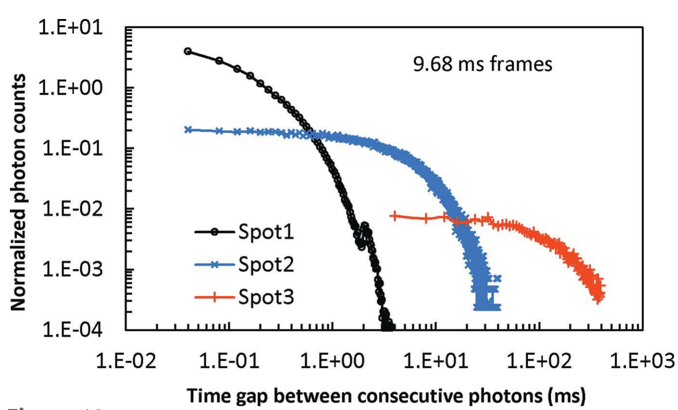

Figure 13
Histogram of the time difference between two consecutive photons in Spots 1–3. Photon counts are normalized by the width of time bins used to produce the histogram: Spots 1 and 2, time bin = 40 µs; Spot 3, time bin = 4 ms. The acquisition sequence with 9.68 ms frame as shown in Fig. 3(*a*).

Files: s/gy5020/gy5020.3d s/gy5020/gy5020.sgml GY5020 FA IU-2113/34(7)5 2110/23(7)5 () GY5020 PROOFS S:FA:2021:28:4:0:0–0

seen in the histogram and is not related to the dynamics of the sample. For Spot 1 the average time gap between photons was ∼63 µs. For each 100 ms period, we introduced an artificial gap of ∼2 ms between consecutive photons due to the particular shutter sequence shown in Fig. 3(*a*). The incoming flux was such that the fraction of photons with 2 ms gaps for Spot 1 was quite low as expected for the 63 µs average time gap. The artificially added 2 ms time gaps constitute a measurable fraction of the events appearing as a bump in our histogram for Spot 1 in Fig. 13. It was washed out in the histogram for Spot 2 where the average time gap between photons was ∼4.1 ms and even longer for Spot 3.

A more detailed view on the local count rate saturation for MCP/Timepix detector is shown in Fig. 14. The saturation of pixels can be effectively considered as a reduction of quantum detection efficiency (QDE) in that area, which changes as a function of time from the start to the finish of the acquisition frame. It is obviously a function corresponding to the frame sequence used during the data acquisition cycle depicted in Fig. 3. The detection efficiency of the brightest Spot 1 is reduced by a factor of 10 compared with the original detector efficiency towards the end of the 9.68 ms frame as seen in Fig.

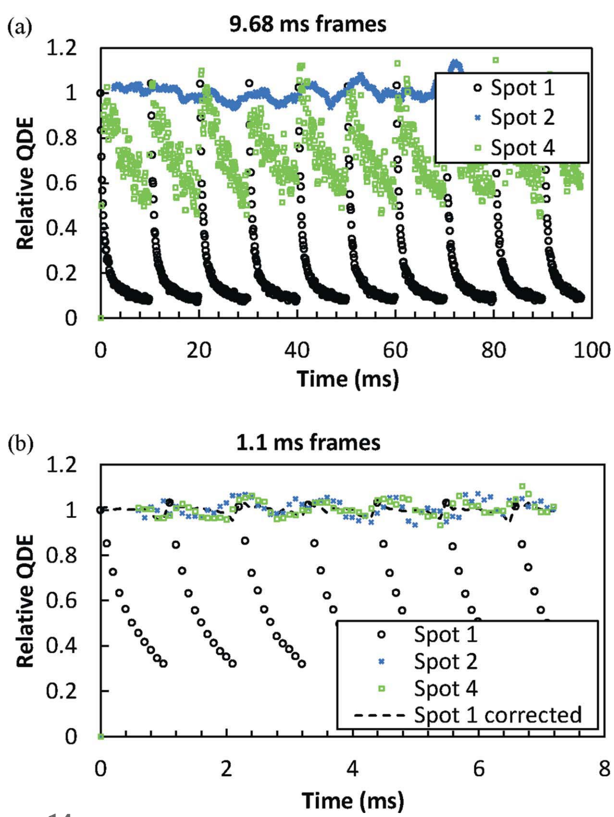

Figure 14
The probability to detect a photon within Spots 1, 2 and 4 varied as a function of time. That probability can be considered as the time-dependent variation of QDE, decreasing within each acquisition frame due to the Timepix one photon per pixel limitation in timing mode. After readout, the probability of detecting a photon is reset to its original value. (*a*) Acquisition frames of 9.68 ms, (*b*) acquisition frames of 1.1 ms showing smaller QDE degradation for bright Spot 1. No QDE degradation is observed for Spot 2 with lower incoming flux. The dashed curve in (*b*) represents the relative QDE variation after correction according to Tremsin *et al.* (2014) and is applied to the raw data.

14(*a*). But for Spot 4, which has ∼17 times lower input flux than spot 1, the probability to detect a photon in that spot is reduced by a factor of 2 towards the end of the acquisition frame. For Spot 2 (∼70 times less intense), it does not show local count rate saturation and subsequently no reduction of detection efficiency. It is obvious from Fig. 14(*b*) that more frequent frame readouts reduce detector saturation and both Spots 2 and 4 do not show any reduction of detection efficiency. Thus 1.1 ms acquisition frames are acceptable for the intensities corresponding to Spots 2, 3 and 4 whereas a 9.68 ms frame can be used only for the intensities lower than that observed in Spot 4.

The local count rate saturation introduced by our detector in some cases can be corrected during data processing, as demonstrated and thoroughly tested in our time-of-flight experiments (Tremsin *et al.*, 2014). The effective reduction of detection efficiency cannot be changed by that data correction, meaning fewer photons are detected and longer acquisition times are required in order to collect sufficient photon counts for a particular analysis. However, the timing characteristics of any quasi-periodic incoming flux could be reconstructed properly by this algorithm. The input flux in many XPCS applications has only small fluctuations above the pulsed structure related to the X-ray source, which is in the sub-10 ns range at most synchrotron sources. Compared with milli-second-wide frames, such flux can be considered as nearly constant as far as the requirements for the correction are concerned. We have not yet proven that XPCS results can be accurately reconstructed for the spots where the detector local count rate saturation modifies the measured photon counts. This will be performed once we have the full XPCS analysis implemented. However, in Fig. 14(*b*) we demonstrate that our data analysis method almost correctly reconstructs the incoming intensity of the oversaturated Spot 1. With longer integration time, this correction becomes even more accurate as the reduction of detection efficiency during the acquisition frame is calibrated more precisely. In short, this correction uses the fact that, for a periodic or constant input signal, the probability a particular pixel is occupied by processing an earlier photon is measured as a function of time from the start of the acquisition frame. With that knowledge, each registered photon can have a correction weight inversely proportional to the probability of the pixel being occupied. More details of this correction technique can be found in the work by Tremsin *et al.* (2014).

5. Conclusions

We demonstrated the strengths and deficiencies of the existing Timepix detection technology for soft X-ray photon counting and imaging experiments. Enabling detection of individual photons using an MCP in combination with the Timepix chip allows us to combine nanosecond time resolution with sustained high count rates. The frame-based readout used in our current detector modulates the timing characteristics of the measured photon flux and introduces substantial limitations on the intensity of measured spots due to localized count

Files: s/gy5020/gy5020.3d s/gy5020/gy5020.sgml **GY5020** FA IU-2113/35(7)5 2110/23(7)5 () GY5020 PROOFS S:FA:2021:28:4:0:0–0

rate saturation. Upgrading to future generations of the Timepix chip will eliminate this problem.

For the current generation of MCP/Timepix detector, optimization of data acquisition parameters, in particular the length of acquisition frames, is needed for a specific scattering pattern. We demonstrated how local count rate saturation can be calibrated before the data are obtained. The use of event-driven Timepix3 and Timepix4 readout chips will eliminate the deficiency of the MCP/Timepix combination detector and should allow the extension of soft XPCS analysis to much faster time scales through photon counting with sub-10 ns timing resolution. Although the temporal resolution of the detector used in our experiments is limited to 10 ns by the Timepix chip internal clock, it will be improved to ~1.6 ns and ~0.2 ns in future generations of MCP detectors with Timepix3 and Timepix4 readouts, respectively. The local count rate capabilities of the Timepix3 readout integrated circuits (ROICs) is 1.3 kHz pixel^{-1} (Poikela *et al.*, 2014) and it is expected to be ~10 kHz pixel^{-1} for Timepix4.

A cluster analysis technique that can be applied to the raw detector data has been developed for the accurate assignment of the correct pixel position of each registered photon, which also improves the spatial resolution of the processed data below the limit of the pixel size. Our experiments demonstrate the capability of MCP detectors to register many near-simultaneous photons with a large dynamic range and virtually no readout noise, helping the ongoing development of next-generation MCP/Timepix detector technology which should extend soft XPCS analysis to nanosecond time scales and improve the resolution of RIXS experiments through event centroiding, facilitating a detector resolution of ~6 µm for the current MCP manufacturing technology.

Funding information

The MCP/Timepix detector used in these experiments was developed at the University of California at Berkeley in collaboration with Techne instruments, Oakland, CA, USA, with great help from the Medipix collaboration, in particular with the help of our colleagues from Advacam s.r.o. and Advacam Oy, the Institute of Experimental and Applied Physics, Czech Technical University in Prague, NiKHEF and the entire team of Medipix/Timepix chip designers at CERN. The work on the MCP/Timepix detector at the University of California was partially funded through the research grants by the US Department of Energy (DOE), National Science Foundation and National Aeronautics and Space Administration. The authors would like to acknowledge the generous donation of the Vertex FPGA and design tools by Xilinx Inc. of San Jose, California, through their Xilinx University Program. The development of the Timepix based soft X-ray detector for correlation spectroscopy is supported by the DOE (award RoyTimepixDetector). This research used resources of the Advanced Light Source, which is a DOE Office of Science User Facility (contract No. DE-AC02-05CH11231). Sample fabrication was supported by the US DOE, Office of Science, Office of Basic Energy Sciences (award No.DE-SC0016519). Use of the Center for Nanoscale Materials, an Office of Science user facility, was supported by the US DOE, Office of Science, Office of Basic Energy Sciences (contract No. DE-AC02-06CH11357). This work was performed in part at the University of Kentucky Center for Nanoscale Science and Engineering and Center for Advanced Materials, members of the National Nanotechnology Coordinated Infrastructure (NNCI), which is supported by the National Science Foundation (contract No. ECCS- 2025075).

References

Becker, J., Bianco, L., Gottlicher, P., Graafsma, H., Hirsemann, H., Jack, S., Klyuev, A., Lange, S., Marras, A. & Rah, S. (2013). *Proceedings of the IEEE Nuclear Science Symposium and Medical Imaging Conference (2013 NSS/MIC)*, 27 October–2 November 2013, Seoul, South Korea. IEEE

Becker *et al.* (2020). **[Please provide the full reference.]**

Bellazzini, R., Spandre, G., Minuti, M., Brez, A., Baldini, L., Latronico, L., Omodei, N., Sgrò, C., Bregeon, J., Razzano, M., Pinchera, M., Tremsin, A. S., McPhate, J. B., Vallerga, J. V. & Siegmund, O. H. W. (2008). *Nucl. Instrum. Methods Phys. Res. A*, **591**, 125–128.

Chen, X. M., Farmer, B., Woods, J. S., Dhuey, S., Hu, W., Mazzoli, C., Wilkins, S. B., Chopdekar, R. V., Scholl, A., Robinson, I. K., De Long, L. E., Roy, S. & Hastings, J. T. (2019). *Phys. Rev. Lett.* **123**, 197202.

Denes, P., Doering, D., Padmore, H. A., Walder, J.-P. & Weizeorick, J. (2009). *Rev. Sci. Instrum.* **80**, 083302.

Dierker, S., Pindak, R., Fleming, R. M., Robinson, I. K. & Berman, L. E. (1995). *Phys. Rev. Lett.* **75**, 449–452.

Fraser, G. W. (1983). *Nucl. Instrum. Methods Phys. Res.* **206**, 265–279.

Galayda, J. N. (2018). *Proceedings of the 9th International Particle Accelerator Conference (IPAC2018)*, 29 April–4 May 2018, Vancouver, BC, Canada, pp. 18–23. IOP.

Graafsma, H., Becker, J. & Gruner, S. M. (2020). *Integrating Hybrid Area Detectors for Storage Ring and Free-Electron Laser Applications.*, pp. 1225–1255. Springer International Publishing.

Grübel, G., Madsen, A. & Robert, A. (2008). *X-ray Photon Correlation Spectroscopy (XPCS)*. In: Borsali R., Pecora R. (eds) *Soft Matter Characterization.*. Dordrecht: Springer.

Hatsuia, T. & Graafsma, H. (2015). *IUCrJ* **2**, 371–383.

Jagutzki, O., Mergel, V., Ullmann-Pfleger, K., Spielberger, L., Spillmann, U., Dörner, R. & Schmidt-Böcking, H. (2002). *Nucl. Instrum. Methods Phys. Res. A*, **477**, 244–249.

Johnson, I., Bergamaschi, A., Buitenhuis, J., Dinapoli, R., Greiffenberg, D., Henrich, B., Ikonen, T., Meier, G., Menzel, A., Mozzanica, A., Radicci, V., Satapathy, D. K., Schmitt, B. & Shi, X. (2012). *J. Synchrotron Rad.* **19**, 1001–1005.

Kleczek, R., Grybos, P., Szczygiel, R. & Maj, P. (2018). *IEEE J.* **53**, 2651–2662.

Llopart, X., Ballabriga, R., Campbell, M., Tlustos, L. & Wong, W. (2007). *Nucl. Instrum. Methods A*, **581**, 485–494.

Martindale, A., Lapington, J. S. & Fraser, G. W. (2007). *Nucl. Instrum. Methods Phys. Res. A*, **573**, 111–114.

Mochrie, S. G. J., Mayes, A. M., Sandy, A. R., Sutton, M., Brauer, S., Stephenson, G. B., Abernathy, D. L. & Grübel, G. (1997). *Phys. Rev. Lett.* **78**, 1275–1278.

Pennicard, D., Lange, S., Smoljanin, S., Hirsemann, H., Graafsma, H., Epple, M., Zuvic, M., Lampert, M. O., Fritzsch, T. & Rothermund, M. (2013). *J. Phys. Conf. Ser.* **425**, 062010.

Poikela, T., Plosila, J., Westerlund, T., Campbell, M., De Gaspari, M., Llopart, X., Gromov, V., Kluit, R., van Beuzekom, M., Zappon, F., Zivkovic, V., Brezina, C., Desch, K., Fu, Y. & Kruth, A. (2014). *JINST*, **9**, C05013.

Files: s/gy5020/gy5020.3d s/gy5020/gy5020.sgml **GY5020** FA IU-2113/35(7)5 2110/23(7)5 () GY5020 PROOFS S:FA:2021:28:4:0:0–0

Rossi, M., Arpaia, R., Fumagalli, R., Moretti Sala, M., Betto, D., Kummer, K., De Luca, G. M., van den Brink, J., Salluzzo, M., Brookes, N. B., Braicovich, L. & Ghiringhelli, G. (2019). *Phys. Rev. Lett.* **123**, 027001.

Rumaiz, A. K., Siddons, D. P., Deptuch, G., Maj, P., Kuczewski, A. J., Carini, G. A., Narayanan, S., Dufresne, E. M., Sandy, A., Bradford, R., Fluerasu, A. & Sutton, M. (2016). *J. Synchrotron Rad.* **23**, 404–409.

Sandy, A. R., Zhang, Q. & Lurio, L. B. (2018). *Annu. Rev. Mater. Res.* **48**, 167–190.

Shpyrko, O. G. (2014). *J. Synchrotron Rad.* **21**, 1057–1064.

Siegmund, O. H. W., Everman, D. E., Vallerga, J. V. & Lampton, M. (1988). *Appl. Opt.* **27**, 1568–1573.

Siegmund, O. H. W., Jelinsky, P., Jelinsky, S., Stock, J., Hull, J., Doliber, D., Zaninovich, J., Tremsin, A. & Kromer, K. (1999). *Proc. SPIE*, **3765**, 429–440.

Siegmund, O. H. W., Tremsin, A. S., Vallerga, J. V., Hull, J. S. & Raffanti, R. (2009). *Proc. SPIE*, **7435**, 74350L.

Sinha, S. K., Jiang, Z. & Lurio, L. B. (2014). *Adv. Mater.* **26**, 7764–7785.

Suhling, K., Airey, R. W. & Morgan, B. L. (1999). *Nucl. Instrum. Methods Phys. Res. A*, **437**, 393–418.

Tremsin, A. S., Lebedev, G. V., Siegmund, O. H. W., Vallerga, J. V., McPhate, J. B. & Hussain, Z. (2007*b*). *Nucl. Instrum. Methods Phys. Res. A*, **582**, 172–174.

Tremsin, A. S., McPhate, J. B., Vallerga, J. V., Siegmund, O. H. W., Bruce Feller, W., Lehmann, E., Kaestner, A., Boillat, P., Panzner, T. & Filges, U. (2012). *Nucl. Instrum. Methods Phys. Res. A*, **688**, 32–40.

Tremsin, A. S. & Siegmund, O. H. W. (2005). *Proc. SPIE*, **5920**, 59200I.

Tremsin, A. S., Siegmund, O. H. W., Hull, J. S., Vallerga, J. V., McPhate, J. B., Soderstrom, J., Chiou, J. W., Guo, J. & Hussain, Z. (2007*a*). *IEEE Trans. Nucl. Sci.* **54**, 706–709.

Tremsin, A. S. & Vallerga, J. V. (2020*b*). *Radiat. Meas.* **130**, 106228.

Tremsin, A. S., Vallerga, J. V., McPhate, J. B. & Siegmund, O. H. W. (2014). *JINST*, **9**, C05026.

Tremsin, A. S., Vallerga, J. V., McPhate, J. B. & Siegmund, O. H. W. (2015). *Nucl. Instrum. Methods Phys. Res. A*, **787**, 20–25.

Tremsin, A. S., Vallerga, J. V. & Raffanti, R. R. (2018). *JINST*, **13**, C11005.

Tremsin, A. S., Vallerga, J. V. & Siegmund, O. H. W. (2020*a*). *Nucl. Instrum. Methods Phys. Res. A*, **949**, 162768.

Vallerga, J., McPhate, J., Tremsin, A., Siegmund, O., Mikulec, B. & Clark, A. (2005). *Nucl. Instrum. Methods Phys. Res. A*, **546**, 263–269.

Vallerga, J. V., Tremsin, A. S., Raffanti, R. & Siegmund, O. H. W. (2011). *Nucl. Instrum. Methods Phys. Res. A*, **633**, S255–S258.

Va'vra, J., Leith, D. W. G. S., Ratcliff, B., Ramberg, E., Albrow, M., Ronzhin, A., Ertley, C., Natoli, T., May, E. & Byrum, K. (2009). *Nuc. Instrum. Methods A* **606**, 404–410.

Vredenborg, A., Roeterdink, W. G. & Janssen, M. H. M. (2008). *Rev. Sci. Instrum.* **79**, 063108.

Westermeier, F., Zozulya, A. V., Bondarenko, S., Parenti, A., Lohmann, M., Schavkan, A., Grübel, G. & Sprung, M. (2013). *J. Phys. Conf. Ser.* **425**, 202005.

Wiza, J. L. (1979). *Nucl. Instrum. Methods*, **162**, 587–601.

Woods, J., Chen, X., Chopdekar, R. V., Farmer, B., Mazzoli, C., Koch, R., Tremsin, A. S., Hu, W., Scholl, A., Kevan, S., Wilkins, S., Kwok, W.-K., De Long, L. E., Roy, S. & Hastings, J. T. (2021). *Phys. Rev. Lett.* **126**, 117201.

Zhang, Q., Dufresne, E. M., Grybos, P., Kmon, P., Maj, P., Narayanan, S., Deptuch, G. W., Szczygiel, R. & Sandy, A. (2016). *J. Synchrotron Rad.* **23**, 679–684.

Zhang, Q., Dufresne, E. M., Narayanan, S., Maj, P., Koziol, A., Szczygiel, R., Grybos, P., Sutton, M. & Sandy, A. R. (2018). *J. Synchrotron Rad.* **25**, 1408–1416.

Files: s/gy5020/gy5020.3d s/gy5020/gy5020.sgml GY5020 FA IU-2113/35(7)5 2110/23(7)5 () GY5020 PROOFS S:FA:2021:28:4:0:0–0

JOURNAL OF SYNCHROTRON RADIATION

ISSN: 1600-5775

ORDER FORM

YOU WILL AUTOMATICALLY BE SENT DETAILS OF HOW TO DOWNLOAD AN ELECTRONIC REPRINT OF YOUR PAPER, FREE OF CHARGE. PRINTED REPRINTS MAY BE PURCHASED USING THIS FORM.

Please scan your order and send to tw@iucr.org

INTERNATIONAL UNION OF CRYSTALLOGRAPHY
5 Abbey Square
Chester CH1 2HU, England.

VAT No. GB 161 9034 76

Article No.: S210390-GY5020

Title of article Photon-counting MCPTimepix detectors for soft X-ray imaging and spectroscopic applications

Name Anton S. Tremsin

Address Space Sciences Laboratory, University of Kentucky, Lexington, KY 40506, USA

E-mail address (for electronic reprints) ast@ssl.berkeley.edu

OPEN ACCESS

IUCr journals offer authors the chance to make their articles open access on **Crystallography Journals Online**. If you wish to make your article open access please go to https://scripts.iucr.org/openaccess/?code=GY5020

The charge for making an article open access is from **1600 United States dollars** (for full details see https://journals.iucr.org/s/services/openaccess.html). For authors in European Union countries, VAT will be added to the open-access charge.

DIGITAL PRINTED REPRINTS

I wish to order . . . . paid reprints

These reprints will be sent to the address given above. If the above address or e-mail address is not correct, please indicate an alternative:

PAYMENT (REPRINTS ONLY)

Charge for reprints . . . . USD

☐ An official purchase order made out to **INTERNATIONAL UNION OF CRYSTALLOGRAPHY** ☐ is enclosed ☐ will follow

Purchase order No.

☐ Please invoice me

☐ I wish to pay by credit card

EU authors only: VAT No:

Date | Signature

OPEN ACCESS

The charge for making an article open access is from **1600 United States dollars** (for full details see https://journals.iucr.org/s/services/openaccess.html). For authors in European Union countries, VAT will be added to the open-access charge.

DIGITAL PRINTED REPRINTS

An electronic reprint is supplied free of charge.

Printed reprints without limit of number may be purchased at the prices given in the table below. The requirements of all joint authors, if any, and of their laboratories should be included in a single order, specifically ordered on the form overleaf. All orders for reprints must be submitted promptly.

Prices for reprints are given below in **United States dollars** and include postage.

	Size of paper (in printed pages)				
Number of reprints required	1–2	3–4	5–8	9–16	Additional 8's
50	184	268	372	560	246
100	278	402	556	842	370
150	368	534	740	1122	490
200	456	664	920	1400	610
Additional 50's	86	128	178	276	116

PAYMENT AND ORDERING

Open-access fees should be paid at https://scripts.iucr.org/openaccess/?code=GY5020

Official purchase orders should be made out to **INTERNATIONAL UNION OF CRYSTALLOGRAPHY**.

Orders should be returned by email to tw@iucr.org

ENQUIRIES

Enquiries concerning reprints should be sent to support@iucr.org.